Sixth International Meeting
on
Wind Turbine Noise
Glasgow 20-23 April 2015

Prediction of infrasound and low frequency noise propagation for modern wind turbines – a proposed supplement to ISO 9613-2

Kristy L. Hansen - Flinders University, Sturt Rd., Bedford Park 5042, SA, Australia. kristy.hansen@flinders.edu.au

George Hessler - Hessler Associates, Inc., 3862 Clifton Manor Place, Suite B Haymarket, VA 20169, USA. George@HesslerAssociates.com

Colin H. Hansen - University of Adelaide, North Tce., Adelaide, 5005, SA, Australia. colin.hansen@adelaide.edu.au

Branko Zajamsek - University of New South Wales, Sydney, 2052, NSW, Australia. b.zajamsek@unsw.edu.au

Summary

A number of propagation models of varying complexity have been developed for environmental noise predictions. While more complex models are correspondingly more accurate, the continued widespread use of the simpler ISO 9613-2 model suggests that its relative simplicity is valued highly. Therefore, to extend the use of ISO 9613-2, it is proposed that a correction should be added to take into account that at some distance from a point source, the propagation of low frequency noise may begin to decay at a rate of 3 dB per doubling of distance rather than 6 dB, during atmospheric conditions where the sonic velocity near the ground increases with altitude, resulting in downward refraction of sound rays and reduced attenuation with distance. Since low frequency sound is poorly attenuated by the ground and atmosphere, a distance from the source will exist beyond which multiple sound rays, which have been reflected from the ground more than once, can arrive at the receiver thereby increasing the sound pressure level at that location. There is some disagreement as to the transition distance at which the attenuation rate changes from 6 dB/doubling of distance to 3 dB, due to the influence of source height, frequency, and the strength of the wind and temperature gradients. This study aims to determine whether decay rates of 3 dB/doubling of distance are applicable to modern wind turbine noise propagation for a range of atmospheric conditions and frequencies and to determine a typical transition distance for the investigated conditions. This investigation focuses on comparison between ISO-9613-2 predictions using different transition distances and a large data set that has been collected at a number of different locations in the vicinity of a modern wind farm. A theoretical analysis is also carried out to calculate the radii of curvature of rays that leave the source at different angles. This enables prediction of the transition distance for various wind profiles and source heights.

1. Introduction

1.1. Current propagation models

A number of sound propagation models have been developed for calculating the attenuation of sound during outdoor propagation. The available models are characterised by varying degrees of complexity, where the more complicated models such as Nord2000 give the most accurate results for prediction of wind turbine noise (Plovsing and Kragh 2006a, 2006b and Plovsing, 2014). On the other hand, these more complicated models require additional input variables that are sometimes not measurable using standard instrumentation. In many cases, existing regulations do not provide enough details with respect to atmospheric velocity and temperature profiles to which they apply and these are required inputs for more advanced models such as Nord2000 and Harmonoise. Determining the relevant terrain profiles, which are required inputs for the more advanced models, also adds a considerable level of complexity. These latter models are also computationally expensive and the end user needs to have a good understanding of the underlying scientific principles in order to obtain meaningful results. Therefore, models with reduced complexity such as ISO 9613-2 and CONCAWE are still widely used for wind farm noise predictions, despite their limitations.

The improved accuracy of more complex models is obtained through a number of additional considerations that have been included in the model description. For example, calculation of the ground effect takes into account the phase angle between the direct and reflected sound waves as well as other effects such as turbulence and frequency band averaging that reduce the coherence between direct and ground reflected waves. None of this complexity is considered in simpler models. However, the effect of the phase shift of the ground reflected wave can be minimised using a microphone on a ground plane and then accounting for the 6 dB increase in sound level due to coherent combination of the direct and ground reflected waves.

Meteorological effects are analysed in more detail for complex models and a linearised atmospheric sonic velocity profile, which is a function of both wind speed and atmospheric temperature profiles, is required, thus providing the means to account for conditions that give rise to significant refraction of sound waves. In contrast, models such as ISO 9613-2 specify a range of downwind velocities at a range of heights for which the model is valid (ISO 9613-2, 2012). Terrain effects have been implemented in both Nord2000 and Harmonoise but ISO 9613-2 is valid for relatively flat terrain only. On the other hand, ISO 9613-2 does specify methods for taking barriers into account and therefore, it is possible to approximately model terrain features as barriers. For high noise sources such as wind turbines, the Nord2000 model is valid for propagation distances of several kilometres; however, uncertainty limits are not provided (Plovsing, 2014). The ISO 9613-2 standard specifies an uncertainty of ±3 dB for measurements between 100 m and 1000 m but an estimate of accuracy is not given for distances exceeding 1000 m, nor for source heights exceeding 30 m. The Nord2000 model is valid for third-octave bands from 25 Hz to 10 kHz, whereas ISO 9613-2 only considers octave bands from 63 Hz to 8 kHz.

While, the accuracy of more complex models is superior, the continued widespread use of the ISO 9613-2 method suggests that model simplicity is valued highly. Therefore, to extend the use of ISO 9613-2, a low frequency supplement is proposed, which is based on the observation that at some specific distance from the source, the propagation of low frequency noise begins to decay at a rate of 3dB per

doubling of distance rather than 6 dB, during atmospheric conditions where the sonic velocity near the ground increases with altitude.

1.2. Characteristics of low frequency propagation

The results of an experimental investigation into long-range propagation of low frequency noise were presented by Willshire Jr. (1985) and Willshire and Zorumski (1987). It was shown that low frequency sound was channelled close to the ground in the downwind direction resulting in an attenuation rate of 3 dB per doubling of distance for frequencies below 20 Hz. Predictions of both ray tracing and normal mode theoretical models supported this observation. In the upwind direction, the absence of a shadow zone was noted and the propagating signals indicated a spherical spreading characteristic, resulting in an attenuation of 6 dB/doubling of distance. While this propagation testing was expertly done at a perfect flat and acoustically hard surface test site on similarly sized wind turbines, it should be pointed out that the prototype wind turbines of the time are now obsolete. The units were two-bladed downwind rotor types that generated intense infrasound from disturbed flow entering the blades. It is possible that modern day turbines with three blades ahead of the support tower may not exhibit the same downwind cylindrical spreading demonstrated conclusively by the NASA testing described above.

The reduced attenuation of low frequency sound in the downwind direction has been attributed to atmospheric refraction (Shepherd & Hubbard, 1990). In the downwind direction, the wind speed gradient causes the sound waves to bend towards the ground, whereas in the upwind direction the rays curve upward away from the ground (Hubbard & Shepherd, 2009), as shown in Figure 1. This reduces the attenuation of low frequency noise in the downwind direction but has little effect in the upwind direction. Vertical temperature gradients also give rise to sound speed gradients; however, the effect of the wind speed gradient is generally dominant in the propagation of sound from wind turbines (Hubbard & Shepherd, 2009). The reduction of low-frequency noise attenuation with distance is a result of sound arriving at the receiver after more than one reflection from the ground. The distance from the sound source at which reduced attenuation will begin to occur is a function of the source height as well as the strength of the atmospheric sonic velocity gradient (and the consequent strength of the downward refraction), as this determines the distance from the source at which the receiver will experience the arrival of more than one ground reflected wave. The effect only occurs at low-frequencies for which losses due to ground reflection and atmospheric absorption are negligible. The path length of reflected rays increases as the number of reflections increase and so the amplitude of the sound pressure arriving at the receiver from each reflected ray decreases as the number of reflections increases, until after a certain number of reflections, a particular ray is no longer an important contributor to the sound pressure level at the receiver. It turns out that the sum of all reflected rays results in a decay of the sound field of approximately 3 dB per doubling of distance which is why it is often referred to as “cylindrical spreading”. Of course there is a gradual transition over both decreasing frequency and increasing distance from the source during which the decay rate changes from 6 dB to 3 dB per doubling of distance.

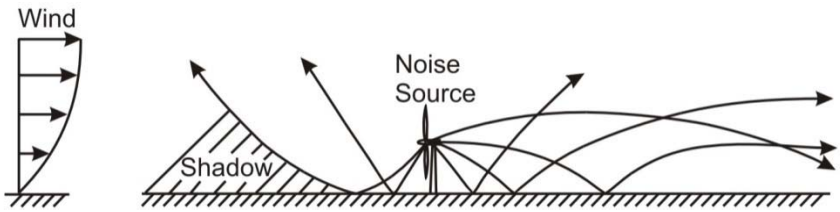

Figure 1 – Schematic showing refraction of sound in downwind direction and formation of a shadow zone in upwind direction.

Another atmospheric condition that is conducive to 3 dB attenuation per doubling of distance is the presence of a low level jet, which gives rise to strong wind and temperature gradients close to the ground. Low level jets are characterised by local wind speed maxima at heights below approximately 500 m (Baas 2008) and they are observed over large flat areas, such as oceans, seas and deserts (Johansson, 2003). It has been found that strong wind and temperature gradients are more prevalent during the night time, due to the presence of atmospheric temperature inversions (André & Mahrt, 1981).

While the occurrence of cylindrical spreading has been observed in a number of studies (Bruce McPherson; Sondergaard & Plovsing, 2005; Boué, 2007) there is some uncertainty as to the distance at which this occurs. A transition distance of 200 m was proposed in the Swedish recommendation for propagation over water (Ljunggren, 1996). While the propagation of sound over hard surfaces will correspond well to that over water for low frequencies, the validity of this result has been questioned (Sondergaard & Plovsing, 2005) since the turbines used in the study were only 20 – 40 m high and only a few data points were collected. According to calculations in their report, Sondergaard and Plovsing (2005) assert that the distance must be larger than 1000 m before multiple reflections become significant. Their results show that the transition distance for wind turbines on short towers (hub height 30 m) begins at distances of 1 – 2 km and for turbines on tall towers (hub height 100 m), the transition distance is approximately 5 km. A number of researchers have proposed distances between these two sets of extreme values but as mentioned by Sondergaard and Plovsing (2005), it is important to consider the height of the noise source above the ground. The results presented by Willshire and Zorumski (1987) suggest that the transition between spherical and cylindrical spreading over land in the downwind direction occurs at approximately 800 m for a wind turbine with an 80 m hub height. The transition distance was found to be 700 m for downwind measurements over sea with a 30 m high synthesised sound source (Boué, 2007). It should be noted that the frequencies under investigation in the Willshire and Zorumski (1987) study were in the range of 5 – 20 Hz, whereas the synthetic sound source in the Boué (2007) study consisted of an 80 Hz speaker source and a 200 Hz compressed-air-driven sound source. Therefore, considering the difference in source heights and the increased atmospheric and ground absorption at higher frequencies, it is conceivable that these studies arrived at a similar result.

It is clear that there is little consensus on the distance at which transition from spherical to cylindrical spreading is believed to occur. This is because the transition distance is dependent on frequency, wind speed and temperature gradients and the hub height of the wind turbines. Nonetheless, it is important to be able predict this transition distance as accurately as possible, since predicted levels can vary by up to 5 dBA for transition distances of 200 m and 700 m, respectively (James, 2012). Therefore, one of the aims of this paper is to determine the approximate transition

distance for low frequency noise propagating from a wind farm. Night time measurements are used exclusively to minimise the influence of extraneous noise sources and also to focus on worst case wind speed and temperature gradients. The propagation characteristics are considered in third-octave bands, which allows investigation of the frequency dependence of the cylindrical spreading characteristic. The wind turbines have a hub height of 80 m, which is common for modern wind turbines. However, the turbines are on hill tops and the height difference between the wind turbines and the residential locations is approximately 100 m. Thus the estimates of transition distance obtained here may be greater than experienced for turbines on flat ground. A large data set is used in the analysis and consists of data collected at several different residences over a period of several weeks.

2. Model to determine transition distance

To determine the point at which the decay rate changes from 6 dB to 3 dB per doubling of distance, the trajectory of multiple sound rays from the wind turbine source to the receiver can be modelled. This modelling requires knowledge of the sonic velocity gradient since this effects the radius of curvature of the sound rays. According to the NORD2000 model (Plovsing and Krugh, 2006b and Plovsing, 2014), the speed of sound, $c(z)$, is calculated as a function of the height, z, above the ground using Equation (1):

$$c(z) = A\log_{\mathrm{e}}\left(\frac{z}{z_0}+1\right) + Bz + C \tag{1}$$

Where $C = c_0$ is the speed of sound at height z = 0, and z_0 is the roughness length of the ground surface, which can vary from 0.0002 for still water to 0.1 for grass. For this study, a conservative value of z_0 = 0.03 was adopted which corresponds to the appropriate value for open flat terrain consisting of grass and a few isolated obstacles. The coefficient, A is determined by the wind speed, $u(z_u)$ at height, z_u, in the direction of propagation and the relation is shown in Equation (2). The standard measurement height is z_u = 10 m and this value has been used in this paper. For the measurements described in Section 5, the maximum velocity at 10 m that occurred between 12 am and 5 am was 6 m/s and this was used as input to Equation (2).

$$A = \frac{u(z_u)}{\log_e\left(\frac{z_u}{z_0}+1\right)} \tag{2}$$

For comparison, a worst case wind profile curve was obtained from SODAR data for which the velocity gradient was most severe. These conditions occurred during the night time on a number of occasions for the field measurements discussed in Section 5. The corresponding equation can be substituted for the first term in Equation (1) and is obtained using a second order polynomial curve fit which is represented in Equation (3)

$$A\log_e\left(\frac{z}{z_0}+1\right) = -0.0003z^2 + 0.1699z + 2.3276 \tag{3}$$

The coefficient, B is a function of the vertical atmospheric temperature gradient, $\mathrm{d}T/\mathrm{d}z$ in ºC/m and the temperature, T at height z in ºC as expressed in Equation (4).

$$B = \frac{\mathrm{d}T}{\mathrm{d}z}\frac{10.025}{\sqrt{T+273.15}} \tag{4}$$

To find the radius of curvature of the various rays, it is necessary to convert the log-lin sound speed profile introduced in Equation (1) to an equivalent linear profile, so that the curved rays will travel along the arc of a circle. The equivalent linear vertical sound speed profile, $c_e(z)$, is calculated using Equation (5) (Plovsing, 2006).

$$c_e(z) = c_0 + \frac{\Delta c}{\Delta z} z \tag{5}$$

The term $\Delta c/\Delta z$ is the average gradient between source and receiver heights, h_S and h_R, respectively, which is calculated according to Equation (6). It should be noted that the source height includes the ridge height in this analysis.

$$\frac{\Delta c}{\Delta z} = \frac{c(h_R) - c(h_S)}{h_R - h_S} \tag{6}$$

The speed of sound at height, z=0 is defined in Equation (7).

$$c_0 = \bar{c} - \frac{\Delta c}{\Delta z}\frac{h_R + h_S}{2} \tag{7}$$

Where, the mean sound speed is given by Equation (8).

$$\bar{c} = \frac{1}{h_R - h_S}\int_{h_S}^{h_R} c(z)\mathrm{d}z \tag{8}$$

The radius of curvature, R for a sound ray leaving at an angle, ψ_S to the horizontal for the case where a hard surface exists between the source and receiver is calculated according to Equation (9).

$$R = \frac{c_o}{\cos\psi_S}\left[\left(\frac{\Delta c}{\Delta z}\right)\right] \tag{9}$$

The distance, d_1 along the ground at which a ray emanating from the source at a specific angle *above* the horizontal, ψ_S will strike the ground can be calculated once the radius of the curvature, R_1 has been calculated. The corresponding relation is determined from geometry and is expressed in Equation (10).

$$d_1 = R_1 \sin\psi_S + R_1 \sin\psi_1 \tag{10}$$

The angle, ψ_2 at which the first ray strikes the ground surface is calculated using Equation (11).

$$\psi_2 = \cos^{-1}(\cos\psi_S - h_S/R_1) \tag{11}$$

The distance between the first reflection and the second reflection is given by Equation (12).

$$d_2 = 2R_2 \sin\psi_2 \tag{12}$$

For the case where the sound ray leaves the source *below* the horizontal at angle, ψ_{1b}, the horizontal distance between the source and the first reflection point, d_{1b}, is determined using Equation (13).

$$d_{1b} = -R_{1b} \sin\psi_{Sb} + R_{1b} \sin\psi_2 \tag{13}$$

The corresponding angle, ψ_2, at which the ray first strikes the ground, is given by equation (14).

$$\psi_2 = \cos^{-1}[\cos\psi_{Sb} - h_S/R_{1b}] \tag{14}$$

Relevant angles and distances are shown schematically in Figure 2.

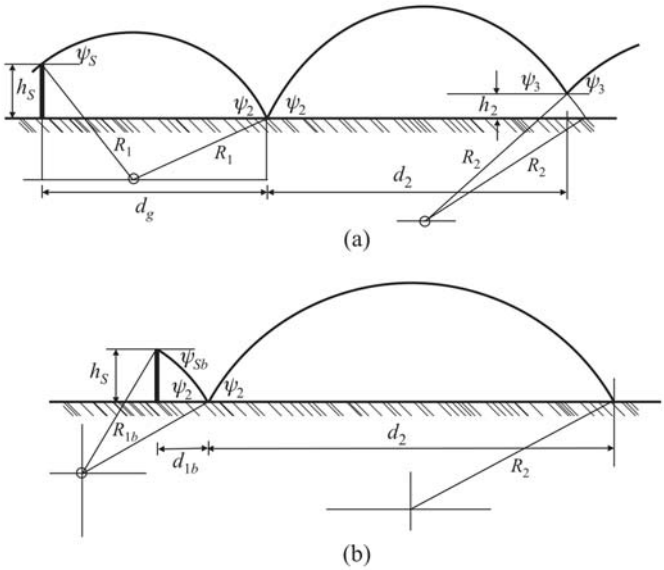

Figure 2 - Geometry for calculating the effect of multiple reflections in a downward refracting atmosphere. (a) Rays emanating from the source above the horizontal. (b) Rays emanating from the source below the horizontal.

The results obtained using this method are presented in Figure 3, where it is shown that the location at which multiple reflections first occurs, varies depending on the specified velocity profile and hence the wind shear gradient. Specifying a wind speed at 10 m height and following the methodology specified in the NORD2000 model (Plovsing and Krugh 2006b and Plovsing, 2014) yields a distance of approximately 5.8 km. Finding the highest wind shear velocity profile obtained from SODAR data and using curve fit data as input to the model gives a distance of approximately 2.9 km. The distance at which multiple reflections first occur corresponds to the point at which 6 dB/doubling of distance is an over-prediction of the attenuation rate. Determining the actual attenuation rate after this point will be the subject of future work. The large difference in predicted transition distance is caused by the effects of the wind speed gradient, which changes the radius of curvature of the rays and hence the points at which they reach the ground.

The ray tracing model was used to determine the variation in the transition distance with source height and the results are compared with published data in Figure 4. Given the large spread in published data, the model indicates reasonable agreement. Differences can be attributed to specification of the sonic velocity profile associated with the measurements. Since this information was not available from the literature, the profile used in this study was specified. The sonic velocity profile has a large impact on the model output, particularly at large propagation distances. This is highlighted in the comparison between results obtained using the velocity profile specified by Nord2000 and the high wind shear profile determined from SODAR data.

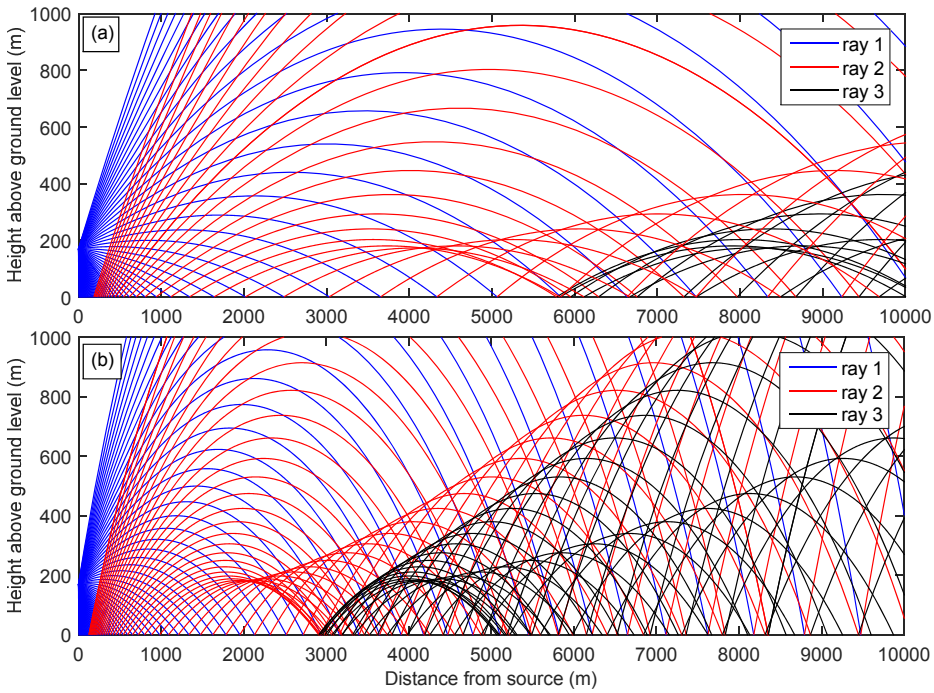

Figure 3 – Results of ray tracing method as calculated for a resolution of 2 degrees for rays leaving the source. Ray 1 corresponds to the ray that leaves the source, ray 2 is the ray that travels from the first to the second reflection point and ray 3 travels from the second to the third reflection point. (a) velocity profile specified by Nord2000 and (b) high wind shear profile determined from SODAR data.

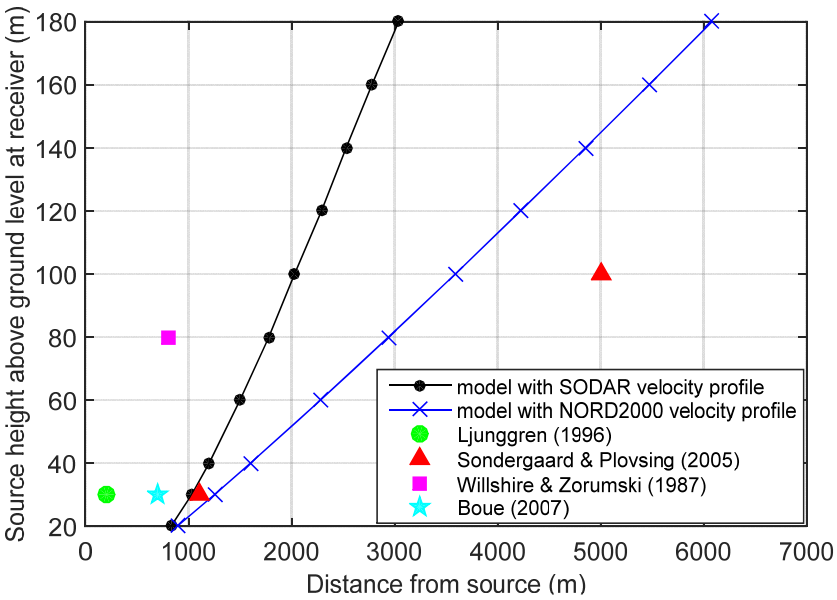

Figure 4 – Comparison between current results and published data for the distance from the source at which multiple ground reflections begin to occur.

3. Sound power measurements

The sound power was determined from overnight measurements taken at two different distances from the Waterloo wind farm as shown in Figure 5. Spherical spreading from the source was assumed and the methodology adopted in the analysis approximately follows the IEC 61400-11 Ed.3 (2012) standard. Deviations from the standard are reported below. The two measurement locations were 177 m and 422 m direct line distance from the nearest wind turbine hub centre. The first location was chosen to

comply with the IEC 61400-11 Ed.3 (2012) standard and the second location was chosen for verification purposes.

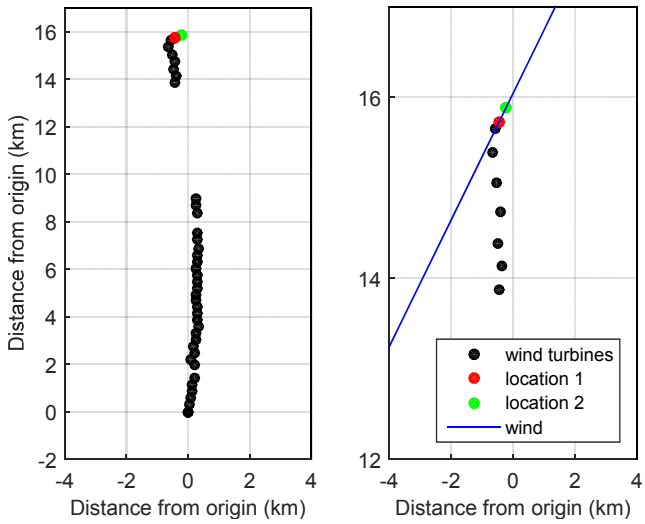

Figure 5 – Layout of wind farm and positioning of microphones and weather stations for three sound power measurement locations. The wind direction was predominantly WSW as shown. The right hand figure is an expanded view of the measurement locations in the left hand figure.

At location 1, the sound pressure level was measured using a single G.R.A.S. type 40AZ microphone with 26CG preamplifier, which has a noise floor of 16 dB(A) and a low frequency linear response down to 0.5 Hz. The microphone was connected to a National Instruments data acquisition device which measured continuous time series data. The microphone was placed on an aluminium ground board and protected by both a 90 mm diameter primary windscreen and a 450 mm diameter hemispherical secondary windscreen. This windscreen arrangement conformed to specifications outlined in the IEC 61400-11 Ed.3 (2012) standard. A Vantage Vue weather station was located nearby at a height of 1 m above the microphone.

At location 2, the microphone, data acquisition system and windshield arrangement were the same as for location 1. An additional G.R.A.S. 40 AZ microphone with SV 12L preamplifier was placed within the windshield and connected to a SVANTEK 958 sound level meter. This instrument measured third-octave data in 10-minute intervals and was used to verify the results measured by the National Instruments system. Also at location 2, a Vantage Vue and a Vantage Pro weather station were located at heights of 1 m and 10 m above the ground, respectively.

The sound pressure level measured at locations 1 and 2 is plotted in Figure 6 and the predicted wind induced noise curves are also plotted for comparison. One of these curves corresponds to data available in the Draft ANSI S12.9 – Part 7 (2014) standard for a ground plane microphone. This data is specific to wind speeds of between 5 and 6 m/s, measured at a height of 1.5 m above the ground, since the mean wind speed at the two locations was within this range. The other curve is derived from the measurements at locations 1 and 2, where the mean wind speed was found to be approximately the same. Three simultaneous equations were developed and solved to determine the rms wind induced sound pressure, *WIN*:

$$x_1^2 + WIN^2 = p_{ref}^2 10^{L_{p1}/10} \tag{15}$$

$$x_2^2 + WIN^2 = p_{ref}^2 10^{L_{p2}/10} \tag{16}$$

$$\frac{x_1^2}{x_2^2} = 10^{\Delta/10} \tag{17}$$

Where, x_1 and x_2 are the rms sound pressures without wind noise at location 1 and 2 respectively, p_{ref} is the reference pressure (20 μPa) and Δ is the difference in levels at locations 1 and 2 assuming spherical spreading and taking into account noise contributions from all turbines. The contribution of wind induced noise is insignificant above 20 Hz and therefore these results are not shown for the calculation in Figure 6. The results indicate that the calculated wind induced noise is generally consistent with Annex C of Draft ANSI S12.9 – Part 7 (2014), except for third-octave frequencies below 3.15 Hz. Therefore, data below 3.15 Hz were not considered in the propagation calculations discussed in Section 4.

The wind induced noise component was determined for each 10-minute measurement based on the wind speed. This component was subsequently subtracted from the corresponding sound pressure level measurement. Due to the large width of the wind speed bins, it was found that this method could result in errors since the predicted wind induced noise was sometimes higher than the measurement. Therefore, values for the wind induced noise component were taken from the adjacent wind speed bin in Annex C of Draft ANSI S12.9 – Part 7 (2014), corresponding to a range 1 m/s lower.

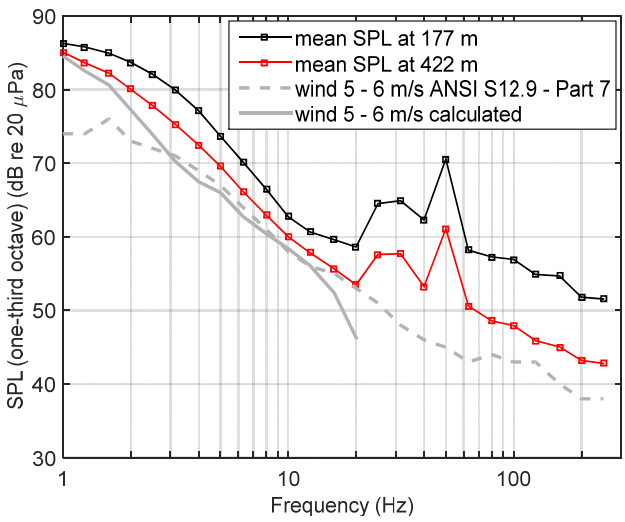

Figure 6 – Sound pressure level measured at locations 1 and 2 and noise level associated with the presence of wind.

The power output data for the Waterloo wind farm are available to the public from the Australian Energy Market Operator (AEMO). These data give the power output for the entire wind farm and therefore in this analysis, it was assumed that each wind turbine generator was producing the same amount of power, as there were no data available for individual wind turbines. Based on these power data, the hub height wind speed was derived from the power curve available from the manufacturer (Vestas, 2006), according to the methodology specified in the IEC 61400-11 Ed.3 (2012) standard. The hub height wind speed range for the measurement period was 8 m/s to 12 m/s, which corresponds to 0.7 to 1 times the wind speed at which the power output is 85%. While this excludes some data required by the IEC 61400-11 Ed.3 (2012) standard at higher wind speeds, conditions of maximum noise generation are included in these results, as will be demonstrated.

To verify the wind speed at hub height as derived from the power output data, data from a SODAR system were also analysed. This device measured wind speed and direction at hub height and was located on the ridge-top in the gap between the Northern and Southern wind turbine group shown in Figure 5. There is reasonable agreement between the wind speeds derived using the turbine output power and measured at hub height, as shown in Figure 7.

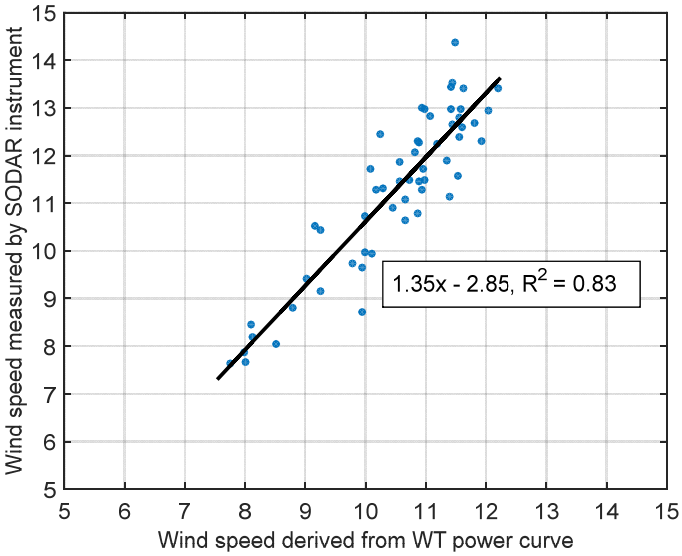

Figure 7 – Comparison between wind speed measured at hub height by the SODAR system and wind speed derived from manufacturer's power curve.

The sound power, L_{WA}, was determined from the measured sound pressure level, L_{Aeq}, using equation (18), which is specified in the IEC 61400-11 Ed.3 (2012) standard.

$$L_{WA} = L_{Aeq} - 6 + 10\log\left(\frac{4\pi R_d^2}{S_0}\right) \tag{18}$$

Where, R_d is the direct line distance between the rotor flange middle point of the wind turbine and the microphone position and S_0 = 1 m^2. The 6 dB is the correction for the pressure doubling effect at the microphone which is caused by coherent interference of the direct and ground reflected waves at the acoustically hard ground board.

Consistent with the IEC 61400-11 Ed.3 (2012) standard, the third-octave sound pressure levels were calculated for time intervals of 10 seconds and the A-weighting was applied in the time domain. The upper frequency limit was limited to 3150 Hz, since analysis of higher frequencies is beyond the scope of this study. Results are compared to the sound power results published in the report by Kaiser-Wilhelm-Koog GmbH (2005) in Figure 8. The hub height wind speeds presented in the figure correspond to the standardised 10 m wind speeds of 6, 7, 8 and 9 m/s respectively.

The analysis was also carried out for data obtained by averaging over blocks of 10 minutes, since this is the relevant averaging time used for compliance measurements at a residence (EPA, 2009). Hence, it was believed that using these data as input for the propagation model would yield more accurate results. The calculated sound power levels for each location are shown in Figure 9 for a hub height wind speed of 11 ± 0.5 m/s. This hub height wind speed is the focus of the analysis in Section 5. The mean spectra were calculated from the measured data for input into the propagation model described in Section 0. The mean sound power values in each third-octave band were calculated using the sound pressure level data measured at Locations 1 and 2 for all frequencies. The contributions of the other turbines in the

wind farm were estimated, based on their distance to the measurement locations, and subtracted from the final result. The mean wind speed at Locations 1 and 2 for hub height wind speeds of 11 ± 0.5 m/s was approximately 5 m/s.

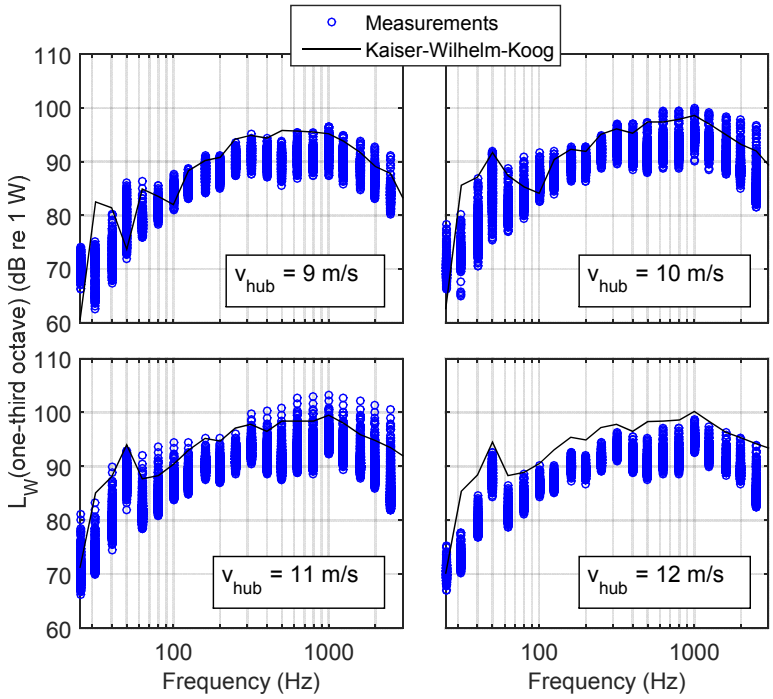

Figure 8 – Comparison of 10-second averaged sound power data from measurements at a horizontal distance of 150 m from the wind turbine, with published data (Kaiser-Wilhelm-Koog GmbH, 2005).

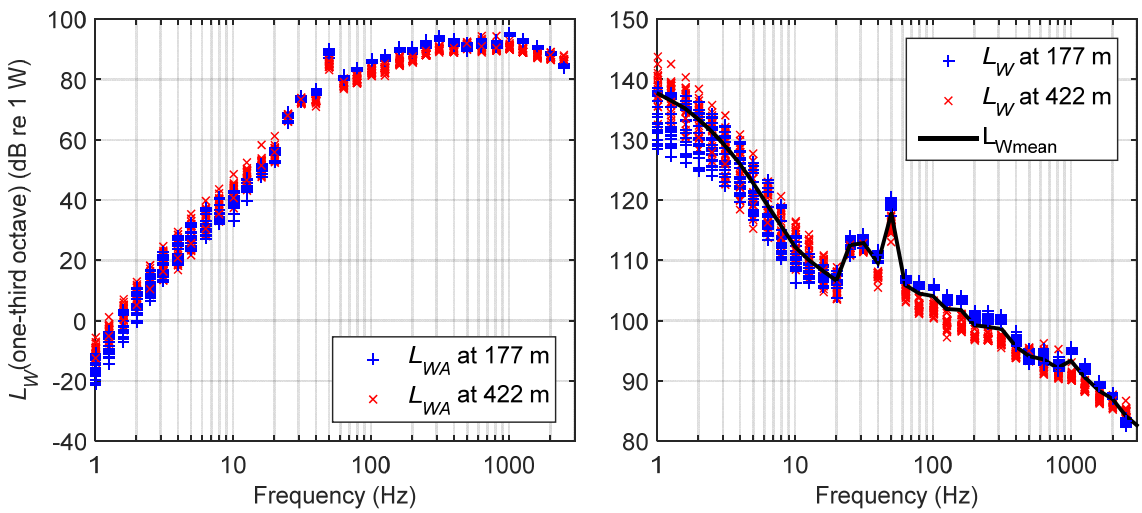

Figure 9 – Measured sound power level averaged over 10-minute intervals for a derived hub height wind speed of 11 ± 0.5 m/s. The left hand figure represents A-weighted data.

The mean third-octave sound power level corresponding to a hub height speed of 11 ± 0.5 m/s is presented in Table 1 for reference.

Table 1 – Mean third-octave sound power level (location 1&2)

Frequency (Hz)	$L_{Wmean,\ 10min}$ (dB re 1 W)	Frequency (Hz)	$L_{Wmean,\ 10min}$ (dB re 1 W)	Frequency (Hz)	$L_{Wmean,\ 10min}$ (dB re 1 W)
2	134	20	107	200	99
2.5	131	25	113	250	99
3.15	129	31.5	113	315	99
4	126	40	110	400	96
5	123	50	118	500	94
6.3	119	63	106	630	94
8	116	80	104	800	92
10	112	100	104	1000	93
12.5	110	125	102		
16	108	160	102		

4. Propagation model

The propagation model is based on the ISO 9613-2 (1996) standard. In the analysis, the sound power output of each wind turbine is assumed to be equal. According to the standard, a number of factors can contribute to attenuation of sound between the source and receiver and these include: geometric spreading of the sound, atmospheric absorption, ground effects, barrier attenuation, vegetation screening and reflections. For this study the relevant attenuation factors are geometric spreading, ground effects and atmospheric absorption.

This model takes into account geometrical spreading by considering results for different distances at which spherical spreading transitions to cylindrical spreading. These results are compared with measured data in Section 5 to determine the most appropriate value for the transition distance. This methodology also takes into account the effect of ground reflections between source and receiver. The ground effect at the receiver is included by adding 6 dB to the predictions, assuming coherent addition of the incoming and reflected waves at the ground-mounted microphone. The attenuation resulting from atmospheric absorption is calculated according to the ANSI S1.26 (2014) standard. The absorption coefficient for the third-octave band centre frequency is used for the entire bandwidth.

5. Field measurements

Continuous outdoor measurements were carried out for periods of approximately one week at four residences located near the Waterloo wind farm, which is made up of 37 operational turbines. The position of these residences with respect to the wind farm is shown in Figure 10 and there is direct line of sight between all turbines and these residences. The outdoor third-octave measurements were made using G.R.A.S. 40AZ / SV 12L microphones connected to a SVAN 958 sound level meter, which measured continuously over 10-minute intervals. The noise floor associated with this instrument and microphone is 17 dB(A). Time series data were measured simultaneously using G.R.A.S. 40AZ / 26CG microphones connected to a National Instruments data acquisition device as described in Section 3. These time series data could be used to check manually for extraneous noise events leading to unexplained variations in spectra.

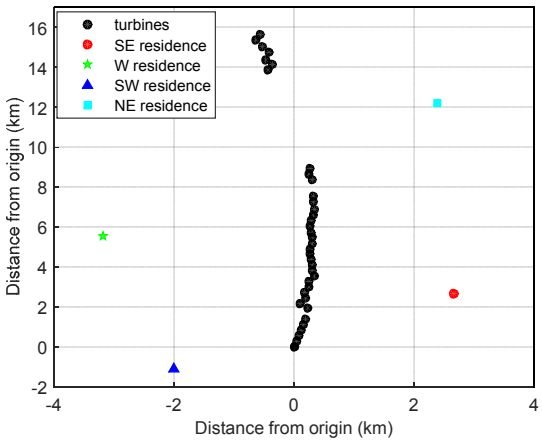

Figure 10 – Position of residences with respect to wind farm.

Hemispherical secondary windshields were used to minimise wind-induced noise experienced by the outdoor microphones, and they were designed to be consistent with the IEC 61400-11 standard, as outlined in Section 3. Wind speed and direction were measured at heights of 1.5 m and 10 m using Davis Vantage Vue and Vantage Pro weather stations, respectively. The weather measurements were collected in 5-minute intervals and then the 10-minute average was calculated during post-processing. Wind speed and direction at hub height were measured using a SODAR unit which was located on the ridge-top in the gap between the Northern and Southern wind turbine group shown in Figure 10. The wind farm operator also provided hub height wind data for the duration of the EPA study and therefore these data are referred to for the W and SW residences in Figure 10. Power output data were accessed from AEMO as described in Section 3.

All of the following results were collected between 12 am and 5 am to minimise interference from extraneous noise sources. As mentioned in Section 3, the focus of this analysis is on hub height wind speeds of 11 ± 0.5 m/s. Also, downwind conditions were considered exclusively. For the W and SW residences, the relevant measurements were determined from hub height wind speed and direction data. As some of the SODAR data were not useable for some measurement times, the hub height wind speed derived from the power curve (Vestas, 2006) was determined only for the SE and NE residences. The wind direction was determined from SODAR data when available and otherwise from 10 m wind data measured at the residence. The number of measurements meeting the wind speed and direction criteria is shown in Table 2 along with other relevant details for each residence.

Table 2 – Distance and direction of residences from nearest Wind Turbine Generator (WTG).

Residence	Distance to nearest WTG (km)	Downwind direction from nearest WTG	Number of 10 min measurements for v_{hub} = 11m/s and downwind	Mean wind speed at 1.5 m (m/s)	Stability: $\frac{\log(v_{hub}/v_{10m})}{\log(h_{hub}/h_{10m})}$
SE	2.4	233 - 323º	13	2.3	0.26 – 0.64
W	3.5	43 - 133º	14	0.2	0.32 – 0.7
SW	2.7	18 - 108º	11	1.0	0.23 – 0.76
NE	3.3	255 - 345º	9	1.8	0.36 – 0.81

Results are shown in Figure 11 to Figure 14 for the four residences depicted in Figure 10 and described in Table 2. The maximum and minimum spectra are shown in each figure and the area between is shaded to indicate the range of measured values. The mean spectra are shown by the red curve, which generally lies midway between the maximum and minimum curves. A line plot has been chosen for clarity but it should be noted that only values at third-octave band centre frequencies are relevant. Also shown on the plots are the predictions obtained using the propagation model described in Section 0. The data points show predictions for spherical spreading only, as well as combined spherical/cylindrical spreading with the transition distance as specified.

In general, the measured data align most closely with the predicted data for frequencies between 8 Hz and 200 Hz. Below 8 Hz the predictions corresponding to spherical spreading are higher than the measured data which suggests that the wind induced noise at these frequencies was higher than predicted for the sound power measurements. Above 200 Hz, the transition distance appears to become smaller than the value for lower frequencies, which is unrealistic. Therefore, this indicates that background noise levels exceed wind turbine noise levels for one third octave bands above 200 Hz at such large distances from the wind farm.

Between 8 Hz and 200 Hz, the alignment of the mean data with predictions varies with location. However, the data generally reflects a combination of spherical/cylindrical spreading with a transition distance from spherical to cylindrical between 1.2 km and 2.4 km. There is no apparent trend in the results which describes the relationship between attenuation characteristics and the third-octave band centre frequency. As mentioned in Section 1.2, it would be expected that low frequency noise would experience reduced attenuation with distance due to a combination of increased downwind refraction and reduced atmospheric absorption. Nonetheless, this characteristic is not clearly represented in the results.

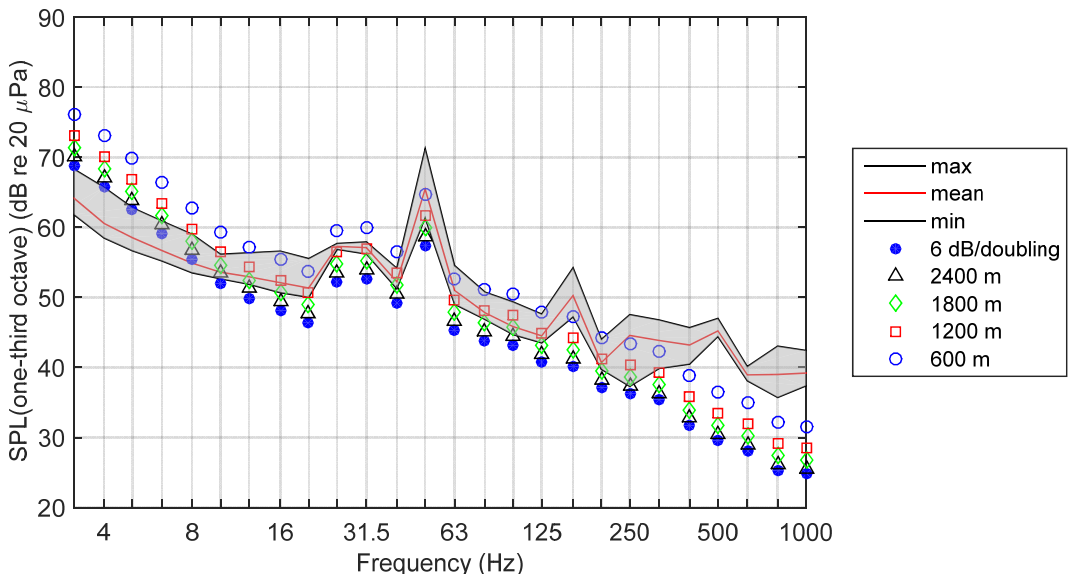

Figure 11 – Comparison between measurements and predictions for the SE residence for various transition distances.

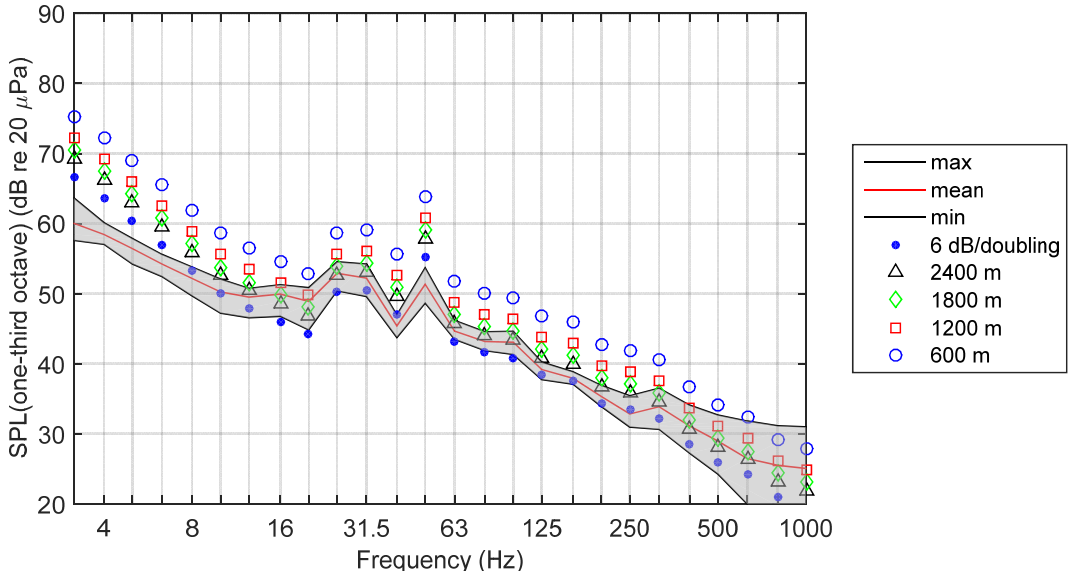

Figure 12 - Comparison between measurements and predictions for the W residence for various transition distances.

The stability characteristics at each residence varied between unstable and stable as shown by the stability factor in Table 2 that was calculated according to Kühner (1998). Therefore, there was no significant difference in the range of stability conditions at the different locations and measurement times. Hence, differences observed in Figure 11 to Figure 14 cannot be explained with reference to stability.

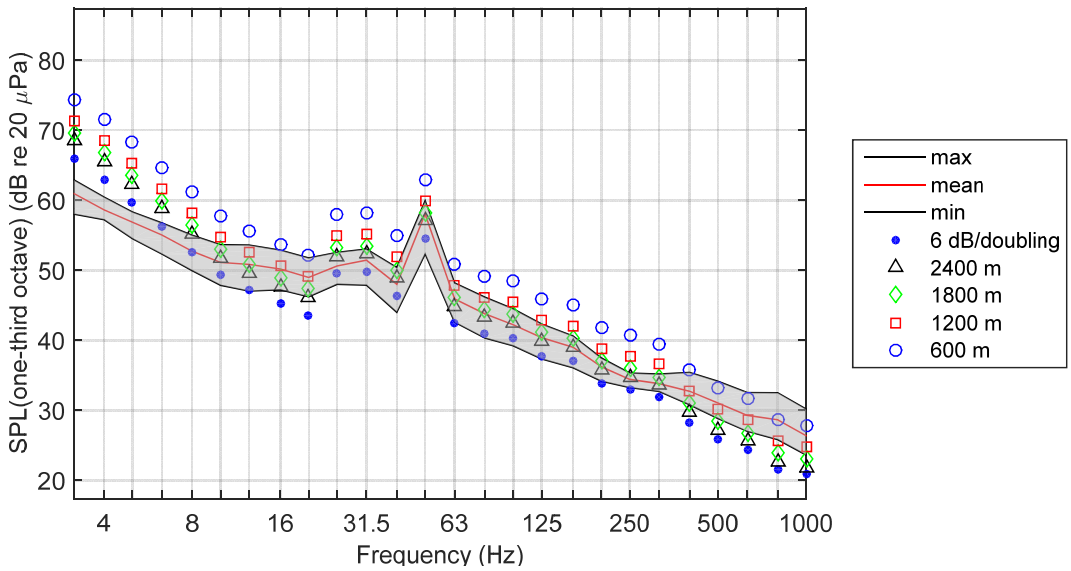

Figure 13 - Comparison between measurements and predictions for the SW residence for various transition distances.

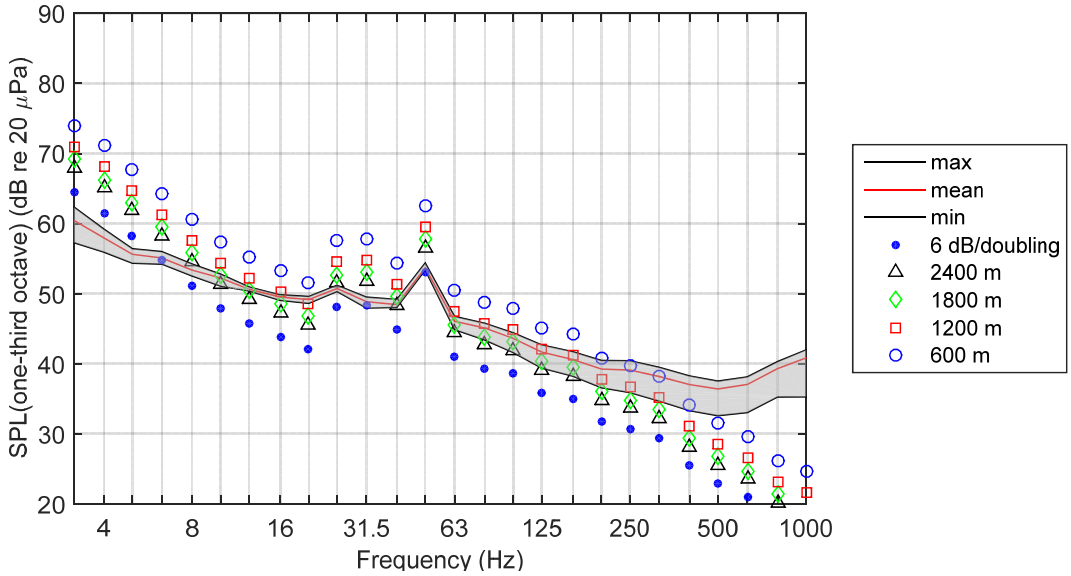

Figure 14 - Comparison between measurements and predictions for NE residence for various transition distances.

6. Discussion/Conclusions

Considering the results obtained from both measurements and theoretical analysis using ray tracing, the data support a combination of spherical and cylindrical spreading for downwind propagation and distances from the wind farm investigated in this study of between 2.4 km and 3.5 km. This result is consistent for all frequencies between 8 Hz and 200 Hz. Below 8 Hz, sound power measurements appeared to be affected by wind induced noise and above 200 Hz, background levels at the residences exceeded wind turbine noise levels. This highlights that at such large distances from the wind farm, low frequency noise below 200 Hz is the dominant wind farm noise source. Hence, research into source characteristics and mitigation strategies should be focussed on these low frequencies in the context of South Australian wind farms.

The distance at which transition from spherical to cylindrical spreading occurs was found to be dependent on the frequency and measurement location. Generally this transition distance lies in the range between 1.2 km and 2.4 km for frequencies between 8 Hz and 200 Hz. This is in reasonable agreement with results obtained using the ray tracing method where the transition distance was predicted to be approximately 2.9 km using a worst case wind profile curve from SODAR data. It should be noted that results presented in this paper are relevant for modern wind turbines of hub height 80 m which are situated on a ridge approximately 100 m high. This is a common situation for South Australian wind farms. It has been shown that the difference between the source and receiver heights is an important variable that will strongly influence the point at which transition from spherical to cylindrical spreading occurs, which is consistent with published literature.

Further analysis could involve consideration of sound power curves for the other hub height wind speeds plotted in Figure 8, for comparison with the data presented in this study which corresponded to an integer hub height wind speed of 11 m/s (± 0.5 m/s). The data sets could be expanded upon through further long-term monitoring to verify the trends presented here. Data could be collected at several locations in the downwind direction simultaneously to ensure that meteorological conditions were consistent for different distances.

To investigate the propagation characteristics for frequencies below 8 Hz, further sound power measurements are required in conditions of high wind shear. This will ensure minimal wind-induced noise at the microphone while at the same time the wind speed at hub height is sufficient for collecting the required sound power data. This is important when comparing propagation model results with measurements at residences for which the local wind speed is very low, as was the case in this study.

References

Ambrose, S. E. and Rand, R. W. (2011), "The Bruce McPherson infrasound and low frequency noise study."

André, J. C. and Mahrt, L. (1982), "The nocturnal surface inversion and influence of clear-air radiative cooling," *Journal of Atmospheric Science*, vol. 39, 864–878.

ANSI/ASA S1.26 (2014), "Methods for calculation of the absorption of sound by the atmosphere," American National Standards Institute.

ANSI S12.9 – Part 7 (draft) (2014), “Measurement of low frequency noise and infrasound outdoors in the presence of wind and indoors in occupied spaces,” American National Standards Institute.

Baas, P., Bosveld, F.C., Klein Baltink, H. and Holtslag, A.A.M. (2009), “A climatology of nocturnal low level jets at Cabauw,” *American Meteorological Society*, vol. 48, pp. 1627 - 1642.

Boué, M. (2007), "Long-range propagation over the sea with application to wind turbine noise," Final report for the Swedish Energy Agency project 21597-3.

Hansen, K.L., Zajamsek, B. and Hansen, C.H. (2013), “Analysis of unweighted low frequency noise and infrasound measured at a residence in the vicinity of a wind farm,” *In Proceedings of Acoustics 2013: Science Technology and Amenity.*

Hubbard, H. H. and Shepherd, K. P. (1991), "Aeroacoustics of large wind turbines," *The Journal of the Acoustical Society of America,* vol. 89, pp. 2495-2508.

Hubbard, H. H. and Shepherd, K. P. (2009), "Wind turbine acoustics," Chapter 7 in D.A. Spera, “Wind turbine technology: fundamental concepts of wind turbine engineering,” ASME, New York.

International standard IEC 61400-11 Ed. 3 (2012), "Wind turbines - Part 11: Acoustic noise measurement techniques," International Electrotechnical Commission.

ISO 9613-2 (R2012), "Acoustics - attenuation of sound during propagation outdoors," International Standards Organisation.

James, R. R. (2012), "Wind turbine infra and low-frequency sound warning signs that were not heard," *Bulletin of Science, Technology & Society,* vol. 32, pp. 108-127.

Johansson, L. (2003), "Sound propagation around off-shore wind turbines: Long-range parabolic equation calculations for Baltic sea conditions,"

Kaiser-Wilhelm-Koog GmbH (2005), "Report of acoustical emissions of a wind turbine generator system of the type V90-3MW, Mode 0 near Bökingharde (Germany)," WINDTEST.

Kühner, D. (1998), "Excess attenuation due to meteorological influence and ground impedance," *Acustica - Acta Acustica,* vol. 84.

Ljunggren, S. (1996), "Ljudutbredning kring havsbaserade vindkraftverk. Resultat fr\aan en litteraturstudie," Department of Civil and Architectural Engineering, KTH, Stockholm.

Plovsing B. and Kragh, J. (R2006), "Nord2000 comprehensive outdoor sound propagation model, Part 1: propagation in an atmosphere without significant refraction," DELTA Acoustics & Vibration Report AV 1849/00.

Plovsing B. and Kragh, J. (R2006), "Nord2000 comprehensive outdoor sound propagation model, Part 2: propagation in an atmosphere with significant refraction," DELTA Acoustics & Vibration Report AV 1851/00.

Plovsing, B. (R2014), "Proposal for Nordtest Method: Nord2000--Prediction of outdoor sound propagation," DELTA Acoustics & Vibration Report AV, vol. 1106/07.

Shepherd K. P. and Hubbard, H. H. (1991), "Physical characteristics and perception of low frequency noise from wind turbines.," *Noise control engineering journal,* vol. 36, pp. 5-15.

Renewable UK (2013), "Wind turbine amplitude modulation: research to improve understanding as to its cause & effect".

SA EPA (2009), "Wind farms environmental noise guidelines," South Australian Environmental Protection Authority.

Vestas (2006), "General specification V90-3MW"

Willshire Jr, W. L. and Zorumski, W. E. (1987), "Low-frequency acoustic propagation in high winds," in *NOISE-CON 87; Proceedings of the National Conference on Noise Control Engineering* vol. 1, pp. 275-280.

Willshire, W. L. (1985), "Long range downwind propagation of low-frequency sound," NASA Technical Memorandam 86409.